Large Eddy Simulation of the Destruction of Convecting Hot Fluid Pockets through a Cold Channel Flow

Z. Saboohi[1*], F. Ommi[1,2], A. Fattahi[3], S. M. Hosseinalipour[4], N. Karimi[5]

[1]Aerospace Research Institute, Ministry of Science Research and Technology, Tehran, Iran

[2]Department of Mechanical Engineering, Tarbiat Modares University, Tehran, Iran

[3]Department of Mechanical Engineering, University of Kashan, Kashan, Iran

[4]School of Mechanical Engineering, Iran University of Science and Technology, Tehran, Iran

[5]School of Engineering, University of Glasgow, Glasgow G12 8QQ, United Kingdom

**corresponding author: zoheir.saboohi@gmail.com*

Abstract

Hot fluid pockets or hot spots can be found in many engineering systems, such as chemical reactors, internal heat engines and gas turbines. They are inherently fluid parcels with rapid temperature rising in comparison with the base medium and usually convect with the flow inertia. Due to the higher energy content, hot fluid pockets can change thermal characteristics of the system. Ignoring the destruction of them, which has been mainly missed in the literature, can therefore change the related predictions. The destruction of the hot fluid pockets is so investigated in this paper using a large eddy simulation and some statistical indices are used to reveal the coherence of the pockets. The results show that the convecting hot pocket can be significantly affected by hydrodynamic and thermal conditions, such that it may loss the initial tempo-spacial distribution completely. The extent of the destruction is various, depending on the flow conditions. The current results will help better prediction for systems involving hot fluid pockets.

Key words: Hot spots, Tempo-spatial destruction, Coherence analysis, Large eddy simulation, fully-developed condition, Cold channel flow.

1. Introduction

Convecting hot fluid pockets may be seen in many engineering applications. Most applicably, they are involved in the physics of chemical reactors, internal heat engines and gas turbines. They are also known as hot spots convecting through the medium by the base flow inertia. Hot spots can change transfer phenomena, due to their high content of energy, which may lead to some non-predictive processes.

In an exothermic chemical reaction, the temperature may continuously increase due to insufficient heat transfer from the walls and reaches to a critical threshold and the abrupt thermal phenomena are then created. This may include a number of convecting hot spots, which can potentially change the reaction rate and locally start a fast chemical progress. Sheu et al. [1] simulated convecting hot spots in a reactive chemical tank, using two-dimensional governing equations of laminar flow and energy field. The hot spots could make the reaction process non-uniform through the reactor. Moving pattern of the spots was under influenced by buoyancy effects. The concentration and temperature of hot spots became oscillatory because of existence of the secondary flow as a cooler and energy production of the reaction as a heater. Similar numerical studies have been carried out with focusing on the production and moving the hot spots [2-6] in chemical reactors, considering critical timescales, for various chemical contents, geometries and boundary conditions with nearly the same conclusions of Ref. [1].

Conevting hot fluid pockets as hot spots are also found in the heat engines due to partial mixing with burned products, heat transfer from hot surfaces, and turbulent energy dissipation in flowing reactants [7]. They are one of the main source of end-combustion auto ignition for undesirable knocking. The important issues related these hot spots are the way of producing and the regimes of burning of them, which have been under consideration of some studies [7-10] often using one-dimensional direct numerical simulation.

Hot fluid pockets or hot spots can play a critical or even vital role in land-based gas turbines or aero-engines. Convecting hot spots in the gas turbine combustor are terminologically called as entropy waves because they are recognizable temperature-time signals with a distinctive velocity [11]. Entropy waves, generated by the unsteady flame, pass through the combustor by the flow inertia. Convection of an entropy wave through a region of mean flow acceleration is a source of sounds in combustive systems, which is correspondingly called entropy noise [12,13]. If entropy waves reach to the outlet nozzle or the first stage

of the gas turbine, the entropy noise can be therefore existed. A part of produced sounds comes back the combustor and so, the entropy waves can be the reason of combustion instability onset. Many efforts have been carried out to avoid combustion instability by the gas turbine manufacturers due to many well-known hazards, such as excessive structural vibration and thermal tension of the combustor, which may cause failure of the power generating system. It is further a source of noise pollution in aero-engines due to propagating the other part of produced sound out of the combustor. Growing demands to have a clean and quiet combustor in both industrial and aeronautic sections have made an increasing interest on entropy waves [14,15]. More than 40 years ago, Ffwocs Williams and Howe [13] showed the potential of the entropy waves to produce sounds. Since then, it has been carried out many attempts for understanding the converting of entropy waves to sounds using analytical [16-19], experimental [20-22] and numerical approaches [23-25].

It is clear that a convecting hot fluid pocket, which inherently is a parcel of irreversibly high temperature, is under diffusing effects of flow field and heat transfer and may become uncorrelated through moving. It is definitely important, because the hot fluid pocket destruction can affect related proceeding occurrences, such as uncontrollable chemical reaction rate or harmful combustion instability in the gas turbines. Nonetheless, there is a little discussion on the hot spots destruction in chemical reactors [26] and also this is nearly missed in the heat engine investigations. The destruction of hot spots is so important to prevent or mitigate in some thermal systems [27,28]. The clue of such destructions in the gas turbines can be found by the controversial conclusions around the entropy wave influence on the combustion instability. In spite of some studies that confirm the contribution of entropy waves in combustor instability of laboratory scale [29,30], there are also some other studies that found no significant effects of the entropy waves on the instability of real scale combustors [31,32]. It is emphasized by Sattelmayer and co-workers in an empirical-analytical work [33] that the entropy waves in the combustors are seriously disappeared by the flow field mixing. On the other hand and by denying the conclusion of Ref. [33], Morgans et al. [34] in a DNS study showed that there is no any energy transfer from the entropy waves and so the annihilation of the wave is negligible. This disagreement in the literature of entropy wave is resulted from unknowing the extent of its

destructions. It was somewhat explained in the numerical work of Hosseinalipour et al. [25]. For the first time. They declared that both preceding viewpoints may be correct; it depends on the hydrodynamic and thermal conditions of the combustor. However, Ref. [25] contains high Reynolds number, which may not be occurred in internal combustion engines or other systems containing hot spots at all. To more investigate the destruction of convecting hot fluid pockets through convection in a channel of lower turbulent Reynolds numbers close to actual conditions, the current work is carried out. Although the current study follows the literature of entropy waves, it also sheds some lights on the behavior of the hot spots in other systems, such as chemical reactors and internal combustion engines. Large eddy simulation is used in a channel consisting of two parallel plates. Common thermal boundary condition of adiabatic walls as well as rarely used convective cooling on the walls is hired to reach real conditions in the channel. Some statistical indices are then used for quantitatively showing the effects of the flow field upon the destruction. It is confirmed that uniform wave front may be completely destroyed in the combustor flow field. It is also found that the wave behavior in lower Reynolds number range is not as regular as that at the higher Reynolds number range. Furthermore, the real thermal boundary conditions of convective heat transfer on the walls can completely change the destruction pattern in comparison to that in the adiabatic combustor.

2. Problem configuration and Numerical method

In this section, geometry, boundary conditions, governing equations, initialization of hot pockets at the channel inlet and validation are discussed.

2.1. Geometry and boundary conditions

Fig. 1 shows a channel consisting of two parallel plates as the geometry similar to those used in the work of Morgans et al. [34]. It presents a computational domain with length, height and width respectively equals $24\pi h$, $2h$ and πh.

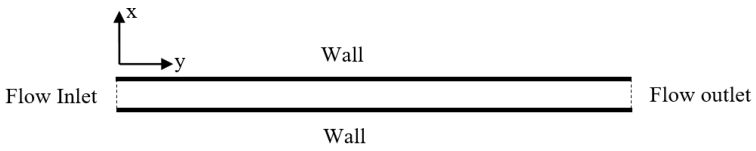

Fig. 1. Schematic side view of the 3D channel; the length, width and height are $24\pi h$, πh and $2h$, respectively.

Reynolds number is considered as 6000 based on hydraulic diameter and bulk velocity. A fully-developed velocity profile at the inlet is applied to keep the longitudinal velocity profile unchanged and exclude it from the influencing parameters. In this work, the flow field in the same channel, which is three times longer than the current channel, was solved and the interest quantities on the last cross section were extracted to map onto the inlet of the main channel [35]. Further, periodic boundary condition in the spanwise direction and no-slip condition on the walls are applied. Zero axial gradients at the outlet for all flow variables are considered as zero [34]. Two distinct thermal boundary conditions, which are adiabatic and convective, are imposed on the walls. The value of the heat transfer coefficient and free stream temperature are 100 W/m^{2}K and 273 K, respectively chosen for external walls of a typical aero combustor [36]. The flow temperature at the inlet is kept constant at 300K and air is assumed as the working fluid.

2.2. Governing equations and numerical methods

Convecting hot fluid pockets or entropy waves are under affecting the flow hydrodynamics [24]. Therefore, flow eddies and their interactions should be precisely detected. Numerical simulation on the basis of Reynolds average Navier-Stokes (RANS) equations cannot capture the realistic behavior of eddies and it may cause incorrect conclusion. Although direct numerical simulation can well capture eddies, it is prohibitively expensive for the current problem. Thus, large eddy simulation (LES) is employed in this study.

Filtering the governing Navier-Stokes equations can effectively recognize the eddy size. This process, like RANS, adds a term to the governing equations, which is unknown. This is called the subgrid-scale stress and requires modeling.

Quantity of φ is decomposed into large-scale $\bar{\varphi}$ and small-scale quantity φ'.

For compressible flows, it is convenient to introduce the density-weighted (or Favre) filtering operator;

$$\tilde{f} = \frac{\overline{\rho f}}{\bar{\rho}}, \tag{1}$$

where the bar denotes the standard LES filtering and ρ the density.

Considering Newtonian fluid and compressible flow, using the Favre averaging, the filtered mass and momentum equations are given by

$$\frac{\partial \bar{\rho}}{\partial t} + \frac{\partial}{\partial x_i}(\bar{\rho}\tilde{u}_i) = 0, \tag{2}$$

$$\frac{\partial}{\partial t}(\bar{\rho}\tilde{u}_i) + \frac{\partial}{\partial x_j}\left(\bar{\rho}\tilde{u}_i\tilde{u}_j\right) = \frac{\partial}{\partial x_j}\left(\tilde{\sigma}_{ij}\right) - \frac{\partial \bar{p}}{\partial x_i} - \frac{\partial \tau_{ij}}{\partial x_j} \tag{3}$$

In Eq. (3), $\tilde{\sigma}_{ij}$ is the stress tensor due to molecular viscosity, defined as

$$\tilde{\sigma}_{ij} = \bar{\mu}\left[\frac{\partial \tilde{u}_i}{\partial x_j} + \frac{\partial \tilde{u}_j}{\partial x_i} - \frac{2}{3}\frac{\partial \tilde{u}_l}{\partial x_l}\delta_{ij}\right], \tag{4}$$

in which ρ, u and p are fluid density, velocity and pressure, respectively. μ is the dynamic viscosity and τ_{ij} is the subgrid-scale stress tensor defined as

$$\tau_{ij} = \bar{\rho}(\widetilde{u_i u_j} - \tilde{u}_i\tilde{u}_j). \tag{5}$$

Based on the Boussinesq hypothesis, the subgrid-scale turbulent stresses are computed as

$$\tau_{ij} - \frac{1}{3}\tau_{kk}\delta_{ij} = -2\mu_t\bar{S}_{ij}, \tag{6}$$

where $\bar{S}_{ij}$ is the strain rate tensor for the resolved scales and defined by

$$\bar{S}_{ij} \equiv \frac{1}{2}\left(\frac{\partial \bar{u}_i}{\partial x_j} + \frac{\partial \bar{u}_j}{\partial x_i}\right) \tag{7}$$

In the current study, Wall-Adapting Local Eddy-Viscosity (WALE) [37] is used to model for subgrid-scale turbulent viscosity (μ_t). This is due to advantages of this model for internal flows, particularly in comparison with the well-known Smagorinsky-Lilly model [38]. Unlike Smagorinsky-Lilly model [38], WALE considers zero turbulent viscosity for laminar shear that makes WALE more correct through the laminar zones. In this model, μ_t is calculated from

$$\mu_t = \rho L_S^2 \frac{\left(S_{ij}^d S_{ij}^d\right)^{3/2}}{\left(\bar{S}_{ij}\bar{S}_{ij}\right)^{5/2} + \left(S_{ij}^d S_{ij}^d\right)^{5/4}}, \tag{8}$$

where $S_{ij}^d = \frac{1}{2}\left(\bar{g}_{ij}^2 + \bar{g}_{ji}^2\right) - \frac{1}{3}\delta_{ij}\bar{g}_{kk}^2$ and $\bar{g}_{ij} = \frac{\partial \bar{u}_i}{\partial x_j}$. L_s is the mixing length of the subgrid-scale and is computed by [37]

$$L_S = min\left(\kappa d, C_w V^{1/3}\right). \tag{9}$$

Details of L_S function can be found in Ref. [37].

The filtered energy equation results in the following equation

$$\frac{\partial \bar{E}}{\partial t} + \frac{\partial}{\partial x_i}\left(\tilde{u}_i(\bar{E} + \bar{P})\right) - \frac{\partial}{\partial x_i}\left(\lambda \frac{\partial \tilde{T}}{\partial x_i}\right) - \frac{\partial}{\partial x_j}\left(\tilde{\sigma}_{ij}\tilde{u}_i\right) + \frac{\partial}{\partial x_j}\left(\overline{Eu_i} - \bar{E}\tilde{u}_i + \overline{pu_i} - \bar{p}\tilde{u}_i\right) = 0, \tag{10}$$

where λ is the thermal conductivity and

$$E = \frac{\rho T}{\gamma} + \rho u_i u_i / 2, \tag{11}$$

in which γ and T are the specific heat ratio and the temperature, respectively.

The governing equations together with the boundary conditions were solved numerically using finite volume method on a Cartesian grid. The unsteady compressible Navier-Stokes and continuity equations are solved simultaneously with the coupled algorithm.

The spatial discretization was performed using the second-order accurate and bounded. A second-order backward Euler transient scheme was applied for the time discretization [39]. To make the Courant-Friedrichs-Lewy number (CFL) [40] lower than unity, the time step value is determined. According to CFL definition, time step is taken to be

$$\Delta t = CFL\, \Delta x_{min} / u_{1\,max}, \tag{12}$$

in which Δx_{min} is the minimum grid width and $u_{1\,max}$ is the maximum longitudinal velocity. A steady RANS simulation was performed to initialize the main solution. Further, to obtain reliable results, a time twice of channel washout of a massless particle is elapsed before recording the results.

2.3. Inlet convecting hot fluid pocket

At the channel inlet, a temperature pulse is introduced as a hot fluid pocket, using a linear increment and an exponential decrement function [20,21]. . This high temperature flow part, with the amplitude of 1.1 times of the base flow temperature (in Kelvin), is then convected by the air flow inertia through the channel. This type of heat source function has the potential of experimental usage [20,21] and lower probable of overshoot numerical error.

2.4. Grid size and validation

To obtain an optimum grid size based on the numerical precision and grid-independent results, various grid sizes were examined. It is found that grid of 490000 cells was sufficiently fine to ensure a grid independent solution. This was checked by LES_IQ_kindex [41] with comparison of this index for various grid sizes. This index is defined as follows.

$$LES\_IQ_k = \frac{k^{res}}{k^{tot}} \tag{13}$$

It is an evaluated index for quality of a LES mesh size. LES_IQ_k for typical internal flow simulation is adequate in the range of 0.75 to 0.85 [41]. Here, $k^{res}$is the resolved kinetic energy and $k^{tot}$is the total kinetic energy. The minimum LES_IQ_k in the current study equals to 91%, which confirms that this cells number assures a grid independency. The grid is further finer near the walls. It is examined by dimensionless velocity (u^+) and wall distance (y^+) for a turbulent flow,

$$u^+ = \frac{U}{u_\tau},\ y^+ = \frac{\rho u_\tau \Delta y}{\mu}, \tag{14}$$

in which Δy is the distance of the cell from the wall and U is the time-averaged velocity. The graph of u^+ versus y^+ in Fig. 2 shows that the current grid ensures a fairly good agreement against DNS results of Moser et al. [42]. Further, y^+ of the nearest cell to the wall is less than unity as recommended by LES developers [43].

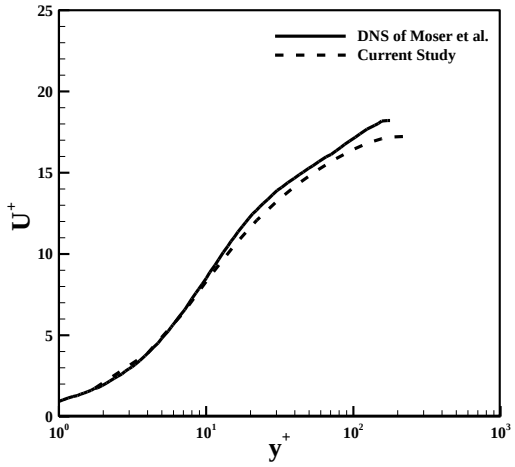

Fig. 2. Dimensionless velocity versus wall distance: a comparison between the current LES and DNS of Moser et al. [40].

For the more validation, the temperature-time pulse, found in Fig. 3, is compared with those of experiment of Bake et al. [20], in which the pulse was produced by a heater module through the cold flow and the temperature is measured by a fast thermocouple. Ref. [20] was only investigated the entropy noise and there was no discussion on the destruction of entropy waves. Due to unknown precise position of the experimental thermocouple in Ref. [20], the presented signal is mass-weighted averaged, which may be the reason behind the differences between two signals at the rear. Except some small differences at the rear of the pulse, good agreement is found in Fig. 3. The current numerical simulation is also compared with DNS of Jongwoo and Yoo [44] regarding the mixed thermal convection. A good coincidence in the velocity and thermal profiles were observed.

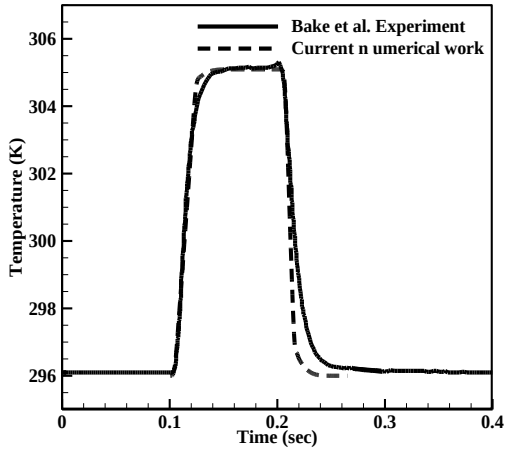

Fig. 3. Temperature increment versus time: a comparison between the current numerical study and experiments of Bake et al. [20].

3. Theoretical Methods

In this section, some relations regarding hot pockets evaluation are introduced.

3.1. Coherence analysis

Every point through the flow field senses a temperature-time sequence as a temporal signal with passing the hot fluid pocket. By calculating the relation between two signals, the destruction can be evaluated. Spectral coherence is a statistic to examine how much two signals or data sets are linearly related. It is a real value that falls between zero and unity; zero value means two signals are completely unrelated, while the unity shows fully linear relation. For two signals of $x(t)$ and $y(t)$, it is defined as

$$C_{xy}(f) = \frac{G_{xy}(f)^2}{G_{xx}(f)G_{yy}(f)}, \tag{15}$$

$G_{xx}(f)$ and $G_{yy}(f)$ are the auto-spectral density of *x* and *y*, respectively, while $G_{xy}(f)$ is the cross-spectral one [45]. They are computed with aiding the definition of mathematical expectation operator [46], defined as

$$E[x(t)] = \int_{-\infty}^{+\infty} x(t)p(t)dt, \tag{16}$$

where $p(t)$ is the probability density function. The spectral densities are then calculated using Fourier transform function, showed by capital letters in the following.

$$G_{xx}(f) = E[X(\omega)X(\omega)],$$
$$G_{xy}(f) = E[X(\omega)Y(\omega)]. \quad (17)$$

The coherence function is calculated for a convecting hot pocket between the inlet and another longitude location. It is also conducted for two points of the pocket front in a cross section. The coherence analyses for former and latter are presented versus Strouhal number, respectively indexed 1 and 2, as follow.

$$St_1 = \frac{f(Hz)}{\frac{U_b}{L}},$$
$$St_2 = \frac{f(Hz)}{\frac{U_b}{h}}, \quad (18)$$

in which U_b is the bulk velocity and L and h are the pipe length and height, respectively.

4. Results and Discussion

It is now well understood that flow hydrodynamics and heat transfer can be a potential to destroy a convecting hot pocket in a high Reynolds turbulent flow [25]. The extent of such destruction, however, is not clear in flows with low Reynolds number for various turbulence contents and thermal conditions. Thus, the flow turbulence intensity and the thermal conditions of the channel are varied during the numerical simulation. Two thermal boundary conditions of adiabatic walls, which is ideal and more common in the studies of combustors, and convective heat transfer on the walls, which is realistic but rarely investigated, are considered. The investigated test cases are listed in Table 1. For all cases, Reynolds number is constant at 6000. In Table 1, TI indicates turbulence intensity. TI is set at the inlet, which may be varied during the system operation by the upstream conditions. This is however modified through the channel by the effects of flow field.

Table 1- Case studies explanation

Case No.	Description
1	TI=5%, Adiabatic walls
2	TI=20%, Adiabatic walls
3	TI=5%, Convective cooling on the walls
4	TI=20%, Convective cooling on the walls

The snapshot of dimensionless temperature ($\Delta T/T_{base}$) for the convecting hot pocket through the channel is depicted in Figs. 4 and 5. The left figures indicate the hot pocket just after complete entrance and the right figures show the pocket just before starting to exit. Higher turbulence intensity of the flow results in a higher deterioration of the hot pocket. It shows with a thinner hot core at the outlet. Near the walls, due to friction and slower velocity, the hot pocket is more annihilated. Further, the convective heat transfer on the walls causes a significant destruction of hot pocket. It causes a decrement in the base flow temperature, as an aggravating factor for pocket annihilating. Thus, the pocket is cooled and subsequently destroyed not only by the cold walls, but also by the cooled base flow.

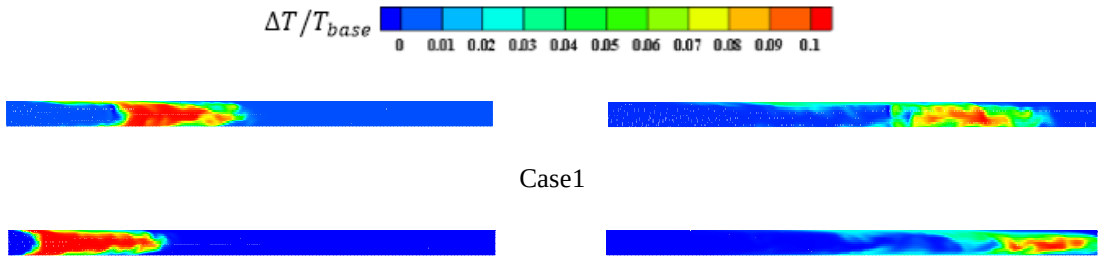

Case1

Case2

Fig. 4. Non-dimensional temperature increment ($\Delta T/T_{base}$) convecting through the channel with adiabatic walls.

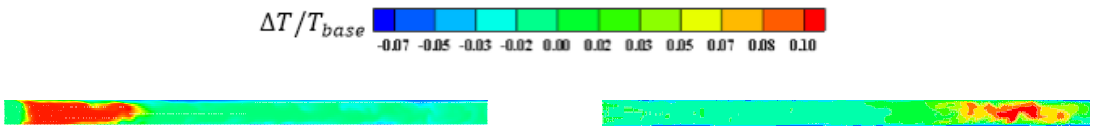

Case3

Case4

Fig. 5. Non-dimensional temperature increment ($\Delta T/T_{base}$) for the hot pocket convecting through the channel with thermally convective cooling on the walls.

Figs. 6 and 7 depict the mass-weighted average variation of $\Delta T/T_{base\ flow}$ during the pocket convection. In these figures, the non-dimensional time is defined as time/(L/U_b) in which L and U_b are the channel length and bulk flow velocity, respectively. Temperature amplitude loss is seen during the pocket convection through the channel in all cases. It is intensified by increasing turbulence intensity. Convection heat transfer on the walls makes a decrement in the base flow temperature causing more cooling for the hot pocket and changing the flow hydrodynamics, which both of them deteriorate the hot pocket. The most reformed shape of the initial hot pocket belongs to case 4, which has the highest turbulence intensity and existence convection heat transfer on the walls. These figures show that turbulence intensity makes a strong effect on shape of the hot pocket. This reveals that eddies energy cascade and contraction between them can definitely reshape the initial pocket. However, by comparing effects of turbulence intensity and convection cooling on the walls, it is inferred that the convection has a stronger influence on the hot pocket than the turbulence intensity, because it affects the pocket by both cooling of the base flow and hydrodynamic changes.

The qualitative behavior of the hot pocket destruction for the current results and those of higher Reynolds number (see Ref. [25]) is similar. However, the quantities show that the hot pocket annihilation by the flow is more emphasized in lower Reynolds number range. The effects of increasing turbulence intensity and convective heat transfer of the walls on the hot pocket are stronger in lower Reynolds number. It shows a lower convecting bulk velocity causes higher deterioration effects upon the hot pocket.

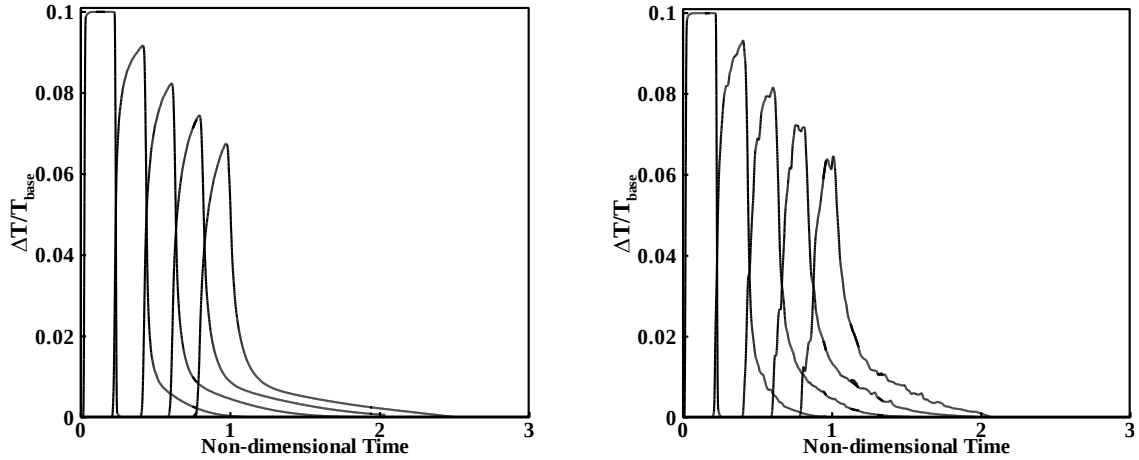

Fig. 6. Variation of the mass-weighted average of $\Delta T/T_{base\ flow}$ during convection of the hot pocket in the adiabatic channel for (a) Case 1 and (b) Case 2

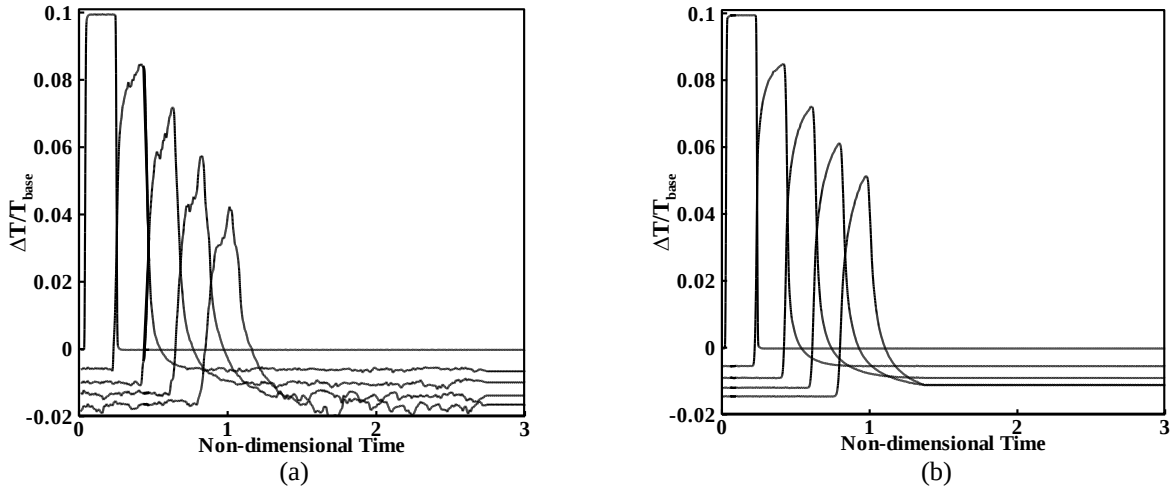

Fig. 7. Variation of the mass-weighted average of $\Delta T/T_{base\ flow}$ during convection of the hot pocket in the heat transferring channel for (a) Case 3 and (b) Case 4.

Coherence of the mass-weighted average of the temperature signal calculated between the inlet and middle of the channel or the channel outlet is shown in Figs. 8 and 9. The longitude coherence is depicted versus Stouhal number indexed 1, defined in Eq. (18). As expected, the pocket remains more coherent between the inlet and middle of the channel compared to the inlet and the outlet. The highest longitude values of coherence belongs to case 1, which has adiabatic walls with the lowest turbulence intensity. Only for case 1, there are some values near unity, meaning a nearly complete coherence. Increasing turbulence intensity in case 2 decreases the coherence. Unlike the cases with high turbulent Reynolds number [25], the high frequencies pretend more coherent trend, which may arise from the complex physics of the flow in the

medium turbulent Reynolds numbers. At the outlet, the coherence of case 2 is near zero, which means a low correlation for the pocket between the inlet and outlet. It also means a considerable destruction in the convecting pocket through the whole channel, due to the hydrodynamic effects. Nevertheless, the coherence depicts a lower destruction at the outlet for case 1 in comparison with that of case 2.

Addition of convective heat transfer on the external walls modifies the coherence of the convecting hot pocket completely. Fig. 9 shows a considerable falling in the coherence for the pocket between the inlet and outlet. The zero values for all frequencies illustrate a complete destruction of the hot pocket through passing the channel. It means at the outlet the pocket's shape and spectrum distribution is entirely different from that at the inlet. It highlights the strongly destructive effects of the cooling of convective heat transfer from walls on the hot pocket. It arises from both thermal and hydrodynamic effects, which cause accelerating non-uniformities in the pocket body. For the coherence between the inlet and middle of the channel, it is also shown mitigated values in comparison with the adiabatic channel. The lowest coherence is found for case 4, which has the convective heat transfer in conjugation with the highest turbulence intensity. Figs. 8 and 9 represent that the convective cooling heat transfer has a more destructive effect on the hot pocket in comparison with increasing turbulence intensity in the studied range.

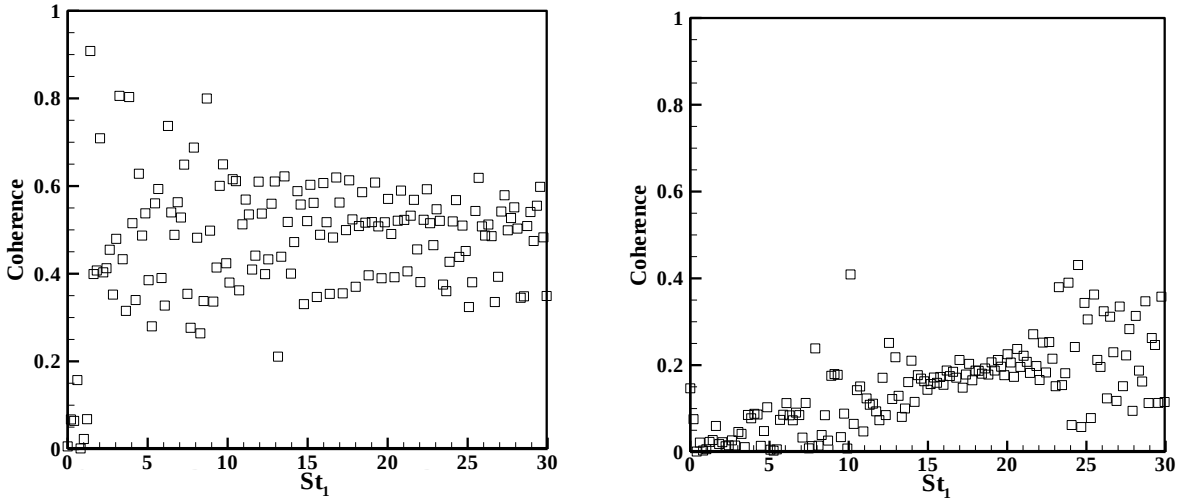

(a)

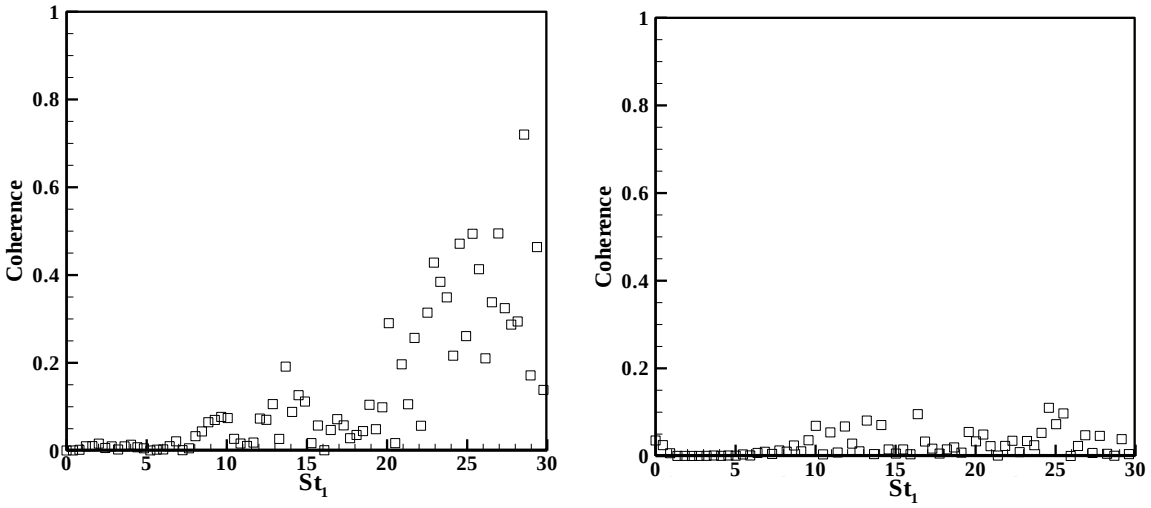

(b)

Fig. 8. Coherence function for the mass-weighted average temperature between inlet and middle (left) and inlet and outlet of the channel (right): (a) Case 1 and (b) Case 2.

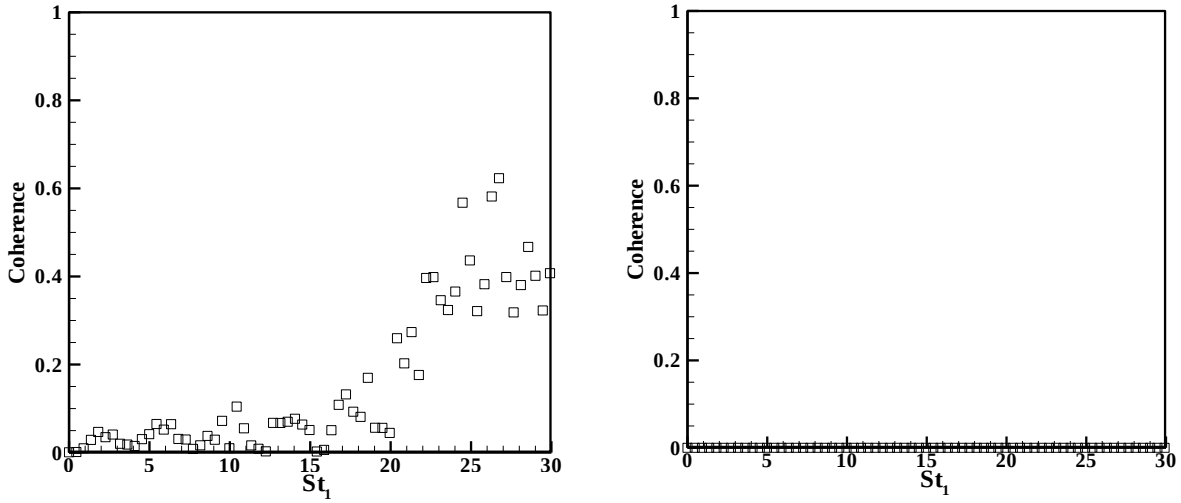

(a)

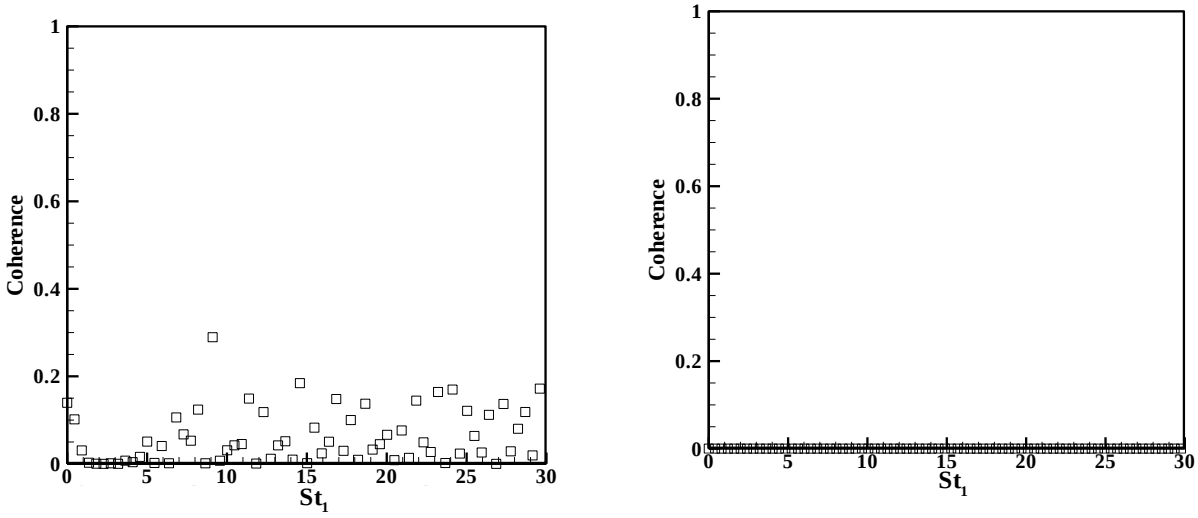

(b)

Fig. 9. Coherence function for the mass-weighted average temperature between inlet and middle of the channel (left) and inlet and outlet of the channel (right): (a) Case 3 and (b) Case 4.

The coherence value on the hot pocket front may be so important, as this presents one-dimensionality of the convecting signal, assumed in some related studies [15,17,19]. It makes modelling of the convecting hot pocket easier, but the validity range of this notion should be evaluated. For this purpose, the coherence between the various points of the pocket front is evaluated. Thus, the coherence between various points on the channel cross section (or the pocket distribution) is investigated here. Three points are considered as Fig. 10 shows. Point 1 is located on the central axis of the channel and the other points are located by the wall with distance of the channel height quarter.

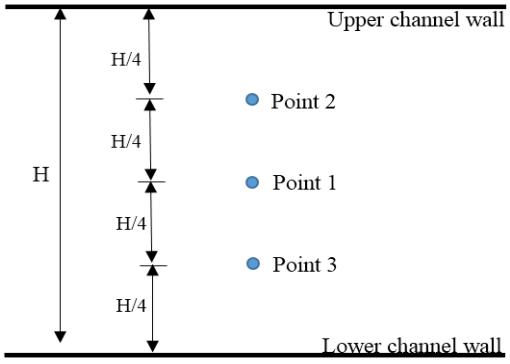

Fig. 10. Points 1-3 on the cross-section of the channel

Fig. 11 shows the coherence function for temperature-frequency signal between points 1 and 2 versus Strouhal number indexed 2, introduced in Eq. (18). The coherence between points 1 and 2 remains unity at about all frequency spectrum at the inlet. By increasing the turbulence intensity for case 2, the coherence falls for values smaller than unity at the high frequencies through the channel inlet. For both cases 1 and 2, the coherence is scattered on the whole spectrum, representing a very weak relation for the signal at middle and outlet of the channel. This trend is also seen for the coherence between points 1 and 3 in Fig. 12. Scattering coherence means that the hot pocket front is completely changed through convecting in the channel. It makes a non-uniform hot front rather than the initial uniform front. These figures illustrate that the adiabatic flow annihilates the hot pocket before it arrives middle of the channel. Although the convecting hot pocket may be initially assumed as a one-dimensional signal, the assumption can be completely violated through convection of the hot pocket.

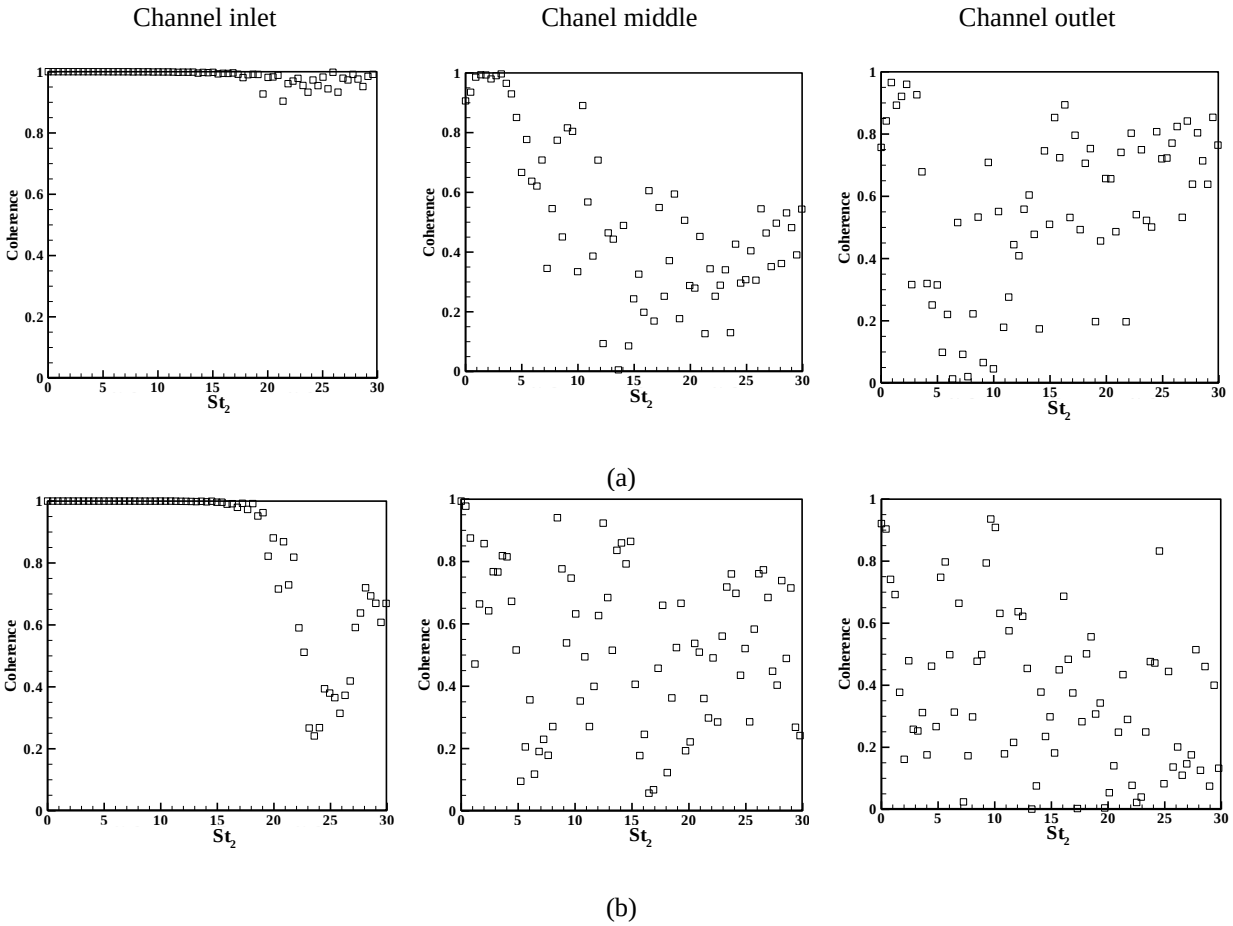

Fig. 11. Coherence function for the temperature-time trend at the inlet, middle and outlet of the channel between points 1&2 for (a) case 1 and (b) case 2.

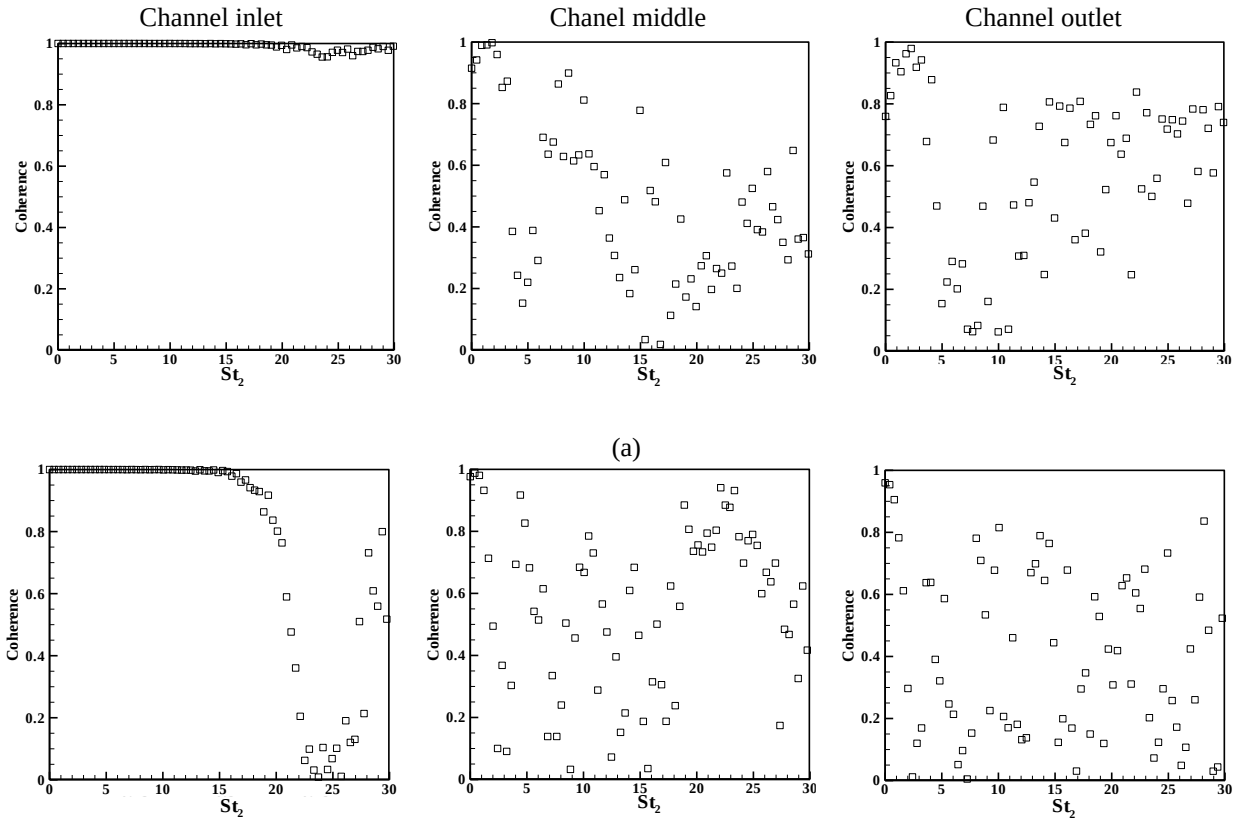

Fig. 12. Coherence function for the temperature-time trend at the inlet, middle and outlet of the channel between points 1&3 for (a) case 1 and (b) case 2.

Addition of convection cooling on the walls makes the coherence lower than that of the adiabatic cases. For case 3 and 4, the signal is deteriorated before middle of the channel, as Figs. 13 and 14 show. At the channel inlet, the coherence is also decreased by increasing the frequency. The signal becomes correlated in the channel inlet at low frequencies (for Strouhal number lower than 10). It was also seen at the adiabatic cases qualitatively, meaning the hot pocket can be importantly one-dimensional only at low frequencies. With enhancing turbulence intensity, the hot pocket is also scattered at the channel inlet. Thus, convecting temperature-time signal exposed to cooling and strong turbulence flow becomes more vulnerable to decay even at the channel inlet. Figs. 13 and 14 demonstrate the correlated signal is rarely found at Reynolds number of 6000 with convective cooling on the walls, except for low turbulence intensity. Comparing the

current results with those of high Reynolds number (see Ref. [25]), it shows a decrement in the Reynolds number results in a serious deterioration upon the hot pocket. The regular trend of signal destruction found in Reynolds number of 6000 is nearly complete different from that seen in the higher Reynolds number [25]. This is raised from the difference between the residence time of two signals, causing more or less effect of the flow field on the hot pocket. Higher residence time not only causes a stronger effect of convective cooling upon the hot pocket and consequently intensified thermal decay, but also presents more opportunity for the flow to affect the hot pocket.

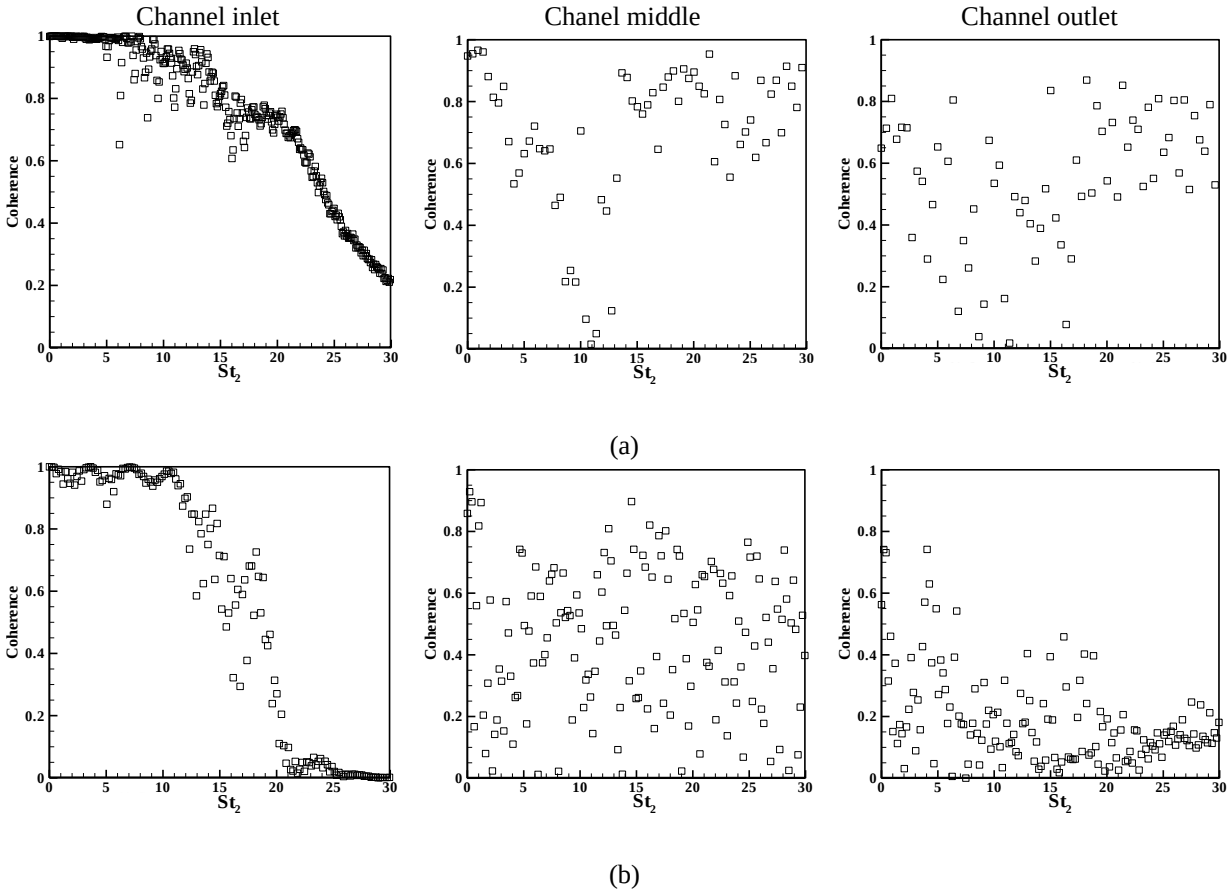

Fig. 13. Coherence function for the temperature-time trend at the inlet, middle and outlet of the channel between points 1&2 for (a) case 3 and (b) case 4.

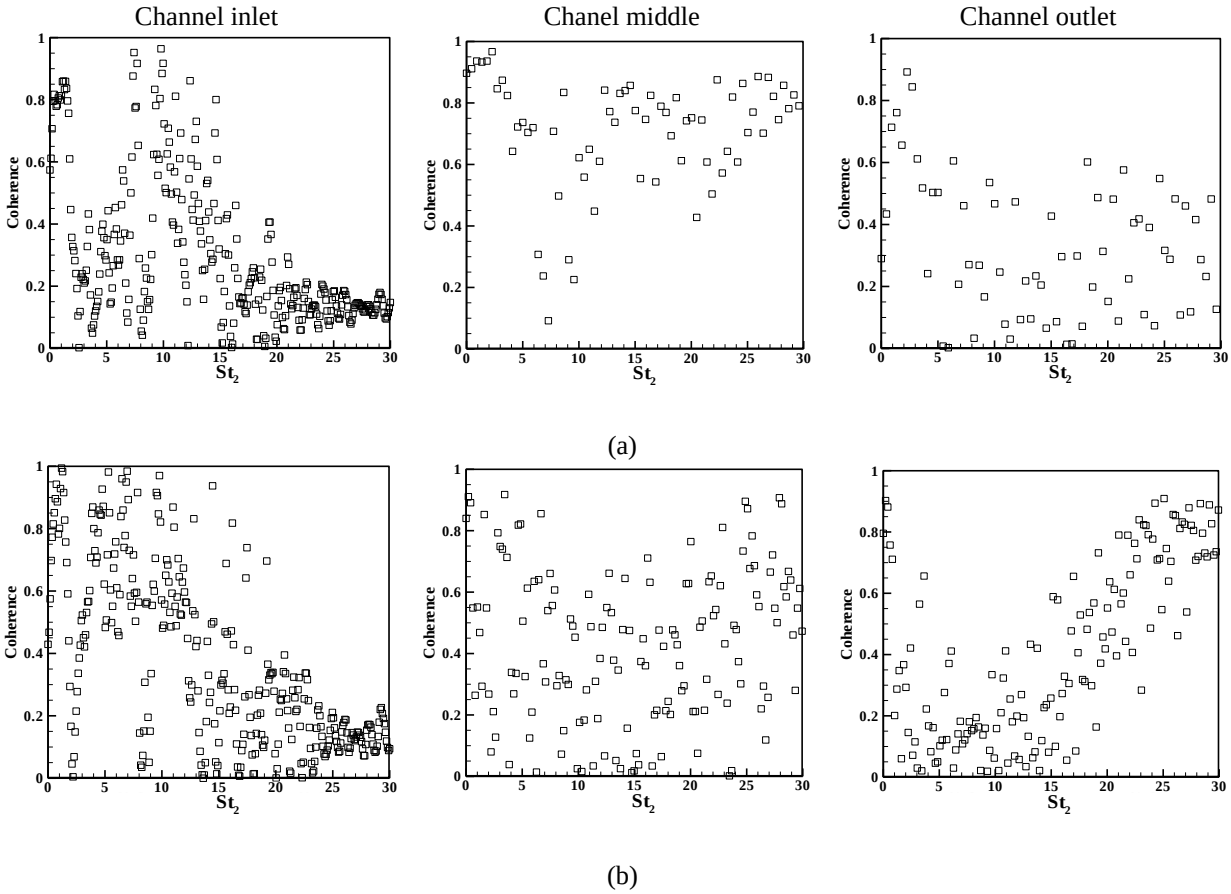

Fig. 14. Coherence function for the temperature-time trend at the inlet, middle and outlet of the channel between points 1&3 for (a) case 3 and (b) case 4.

5. Conclusion

Hot fluid pocket convecting through a flow medium may be found in some engineering applications, such as chemical reactors, internal combustion engines and gas turbines. They can be the onset of some undesirable phenomena; therefore, the probable destruction of the pocket may cancel out or even push related processes. This has been mainly missed in the literature. The destruction of convevting hot fluid pocket was investigated through a large eddy simulation in the current work. The pocket deterioration was more found for lower Reynolds number or higher turbulence intensity. The convective cooling on the channel caused a significant destruction. Using a statistical analysis, the relation between points of the hot pocket on longitude and transverse direction was investigated. The points on the pocket became unrelated in all cases from inlet to outlet of the channel, indicating the effects of the flow and heat transfer on the convecting hot pocket and non-one-dimensional behavior of them. The results confirmed that the

destruction of hot fluid pockets was significant in low turbulent Reynolds number and therefore, it should be considered for the systems of lower velocity.

References

[1] Sheu LJ, Lin JD, Chen JR. Numerical analysis on the hot spot in reactive chemical storage. Journal of loss prevention in the process industries. 1999 Mar 1;12(2):125-36.

[2] Liu TY, Campbell AN, Cardoso SS, Hayhurst AN. Effects of natural convection on thermal explosion in a closed vessel. Physical Chemistry Chemical Physics. 2008;10(36):5521-30.

[3] Chambre PL. On the Solution of the Poisson-Boltzmann Equation with Application to the Theory of Thermal Explosions. The Journal of Chemical Physics. 1952 Nov;20(11):1795-7.

[4] Parks JR. Criticality criteria for various configurations of a self-heating chemical as functions of activation energy and temperature of assembly. The Journal of Chemical Physics. 1961 Jan;34(1):46-50.

[5] Merzhanov AG. On critical conditions for thermal explosion of a hot spot. Combustion and Flame. 1966 Dec 1;10(4):341-8.

[6] Boddington T, Gray P, Harvey DI. Thermal theory of spontaneous ignition: criticality in bodies of arbitrary shape. Phil. Trans. R. Soc. Lond. A. 1971 Dec 2;270(1207):467-506.

[7] Bates L, Bradley D, Paczko G, Peters N. Engine hot spots: Modes of auto-ignition and reaction propagation. Combustion and Flame. 2016 Apr 1;166:80-5.

[8] Terashima H, Matsugi A, Koshi M. Origin and reactivity of hot-spots in end-gas autoignition with effects of negative temperature coefficients: Relevance to pressure wave developments. Combustion and Flame. 2017 Oct 1;184:324-34.

[9] Ju Y, Sun W, Burke MP, Gou X, Chen Z. Multi-timescale modeling of ignition and flame regimes of n-heptane-air mixtures near spark assisted homogeneous charge compression ignition conditions. Proceedings of the Combustion Institute. 2011 Jan 1;33(1):1245-51.

[10] Terashima H, Koshi M. Mechanisms of strong pressure wave generation in end-gas autoignition during knocking combustion. Combustion and Flame. 2015 May 1;162(5):1944-56.

[11] Whitham GB. Linear and nonlinear waves. John Wiley & Sons; 2011 Oct 18.

[12] Lieuwen TC. Unsteady combustor physics. Cambridge University Press; 2012 Aug 27.

[13] Williams JF, Howe MS. The generation of sound by density inhomogeneities in low Mach number nozzle flows. Journal of Fluid Mechanics. 1975 Aug;70(3):605-22.

[14] Miles JH. Time delay analysis of turbofan engine direct and indirect combustion noise sources. Journal of Propulsion and Power. 2009 Jan;25(1):218-27.

[15] Hield PA, Brear MJ, Jin SH. Thermoacoustic limit cycles in a premixed laboratory combustor with open and choked exits. Combustion and Flame. 2009 Sep 1;156(9):1683-97.

[16] Howe MS. Contributions to the theory of aerodynamic sound, with application to excess jet noise and the theory of the flute. Journal of Fluid Mechanics. 1975 Oct;71(4):625-73.

[17] Marble FE, Candel SM. Acoustic disturbance from gas non-uniformities convected through a nozzle. Journal of Sound and Vibration. 1977 Nov 22;55(2):225-43.

[18] Stow SR, Dowling AP, Hynes TP. Reflection of circumferential modes in a choked nozzle. Journal of Fluid Mechanics. 2002 Sep;467:215-39.

[19] Cumpsty NA, Marble FE. Core noise from gas turbine exhausts. Journal of Sound and Vibration. 1977 Sep 22;54(2):297-309.

[20] Cumpsty NA. Jet engine combustion noise: pressure, entropy and vorticity perturbations produced by unsteady combustion or heat addition. Journal of Sound and Vibration. 1979 Oct 22;66(4):527-44.

[21] Bake F, Richter C, Mühlbauer B, Kings N, Röhle I, Thiele F, Noll B. The entropy wave generator (EWG): a reference case on entropy noise. Journal of Sound and Vibration. 2009 Oct 9;326(3-5):574-98.

[22] Bake F, Kings N, Roehle I. Fundamental mechanism of entropy noise in aero-engines: Experimental investigation. Journal of Engineering for Gas Turbines and Power. 2008 Jan 1;130(1):011202.

[23] Talei M, Hawkes ER, Brear MJ. A direct numerical simulation study of frequency and Lewis number effects on sound generation by two-dimensional forced laminar premixed flames. Proceedings of the Combustion Institute. 2013 Jan 1;34(1):1093-100.

[24] Zhu M, Dowling AP, Bray KN. Self-excited oscillations in combustors with spray atomizers. Journal of engineering for gas turbines and power. 2001 Oct 1;123(4):779-86.

[25] Fattahi A, Hosseinalipour SM, Karimi N. On the dissipation and dispersion of entropy waves in heat transferring channel flows. Physics of Fluids. 2017 Aug 28;29(8):087104.

[26] .Liu TY, Campbell AN, Hayhurst AN, Cardoso SS. On the occurrence of thermal explosion in a reacting gas: The effects of natural convection and consumption of reactant. Combustion and Flame. 2010 Feb 1;157(2):230-9.

[27] Patel J, Parekh K, Upadhyay RV. Prevention of hot spot temperature in a distribution transformer using magnetic fluid as a coolant. International Journal of Thermal Sciences. 2016 May 1;103:35-40.

[28] Maganti LS, Dhar P, Sundararajan T, Das SK. Mitigating non-uniform heat generation induced hot spot (s) in multicore processors using nanofluids in parallel microchannels. International Journal of Thermal Sciences. 2018 Mar 31;125:185-96.

[29] Talei M, Brear MJ, Hawkes ER. A comparative study of sound generation by laminar, combusting and non-combusting jet flows. Theoretical and Computational Fluid Dynamics. 2014 Aug 1;28(4):385-408.

[30] Karimi N. Response of a conical, laminar premixed flame to low amplitude acoustic forcing–A comparison between experiment and kinematic theories. Energy. 2014 Dec 15;78:490-500.

[31] Choy YS, Zhen HS, Leung CW, Li HB. Pollutant emission and noise radiation from open and impinging inverse diffusion flames. Applied energy. 2012 Mar 1;91(1):82-9.

[32] Zhen HS, Choy YS, Leung CW, Cheung CS. Effects of nozzle length on flame and emission behaviors of multi-fuel-jet inverse diffusion flame burner. Applied energy. 2011 Sep 1;88(9):2917-24.

[33] Sattelmayer T. Influence of the combustor aerodynamics on combustion instabilities from equivalence ratio fluctuations. Journal of Engineering for Gas Turbines and Power. 2003 Jan 1;125(1):11-9.

[34] Morgans AS, Goh CS, Dahan JA. The dissipation and shear dispersion of entropy waves in combustor thermoacoustics. Journal of Fluid Mechanics. 2013 Oct;733.

[35] Montorfano A, Piscaglia F, Ferrari G. Inlet boundary conditions for incompressible les: A comparative study. Mathematical and Computer Modelling. 2013 Apr 1;57(7-8):1640-7.

[36] Lefebvre AH. Gas turbine combustion. CRC press; 1998 Sep 1.

[37] Nicoud F, Ducros F. Subgrid-scale stress modelling based on the square of the velocity gradient tensor. Flow, turbulence and Combustion. 1999 Sep 1;62(3):183-200.

[38] Smagorinsky J. General circulation experiments with the primitive equations: I. The basic experiment. Monthly weather review. 1963 Mar;91(3):99-164.

[39] Franke J, editor. Best practice guideline for the CFD simulation of flows in the urban environment. Meteorological Inst.; 2007.

[40] Chu BT. On the energy transfer to small disturbances in fluid flow (Part I). Acta Mechanica. 1965 Sep 1;1(3):215-34.

[41] Celik IB, Cehreli ZN, Yavuz I. Index of resolution quality for large eddy simulations. Journal of fluids engineering. 2005 Sep 1;127(5):949-58.

[42] Moser RD, Kim J, Mansour NN. Direct numerical simulation of turbulent channel flow up to Reτ= 590. Physics of fluids. 1999 Apr;11(4):943-5.

[43] Pope SB, Pope SB. Turbulent flows. Cambridge university press; 2000 Aug 10.

[44] You J, Yoo JY, Choi H. Direct numerical simulation of heated vertical air flows in fully developed turbulent mixed convection. International Journal of Heat and Mass Transfer. 2003 Apr 1;46(9):1613-27.

[45] Newland DE. An introduction to random vibrations, spectral & wavelet analysis. Courier Corporation; 2012 Apr 3.

[46] Lindquist EF. Design and analysis of experiments in psychology and education.